Correlation of X-Ray Dark-Field Radiography to Mechanical Sample Properties

Andreas Malecki,[1,2] Elena Eggl,[1,2] Florian Schaff,*[,1,2] Guillaume Potdevin,[1,2] Thomas Baum,[3] Eduardo Grande Garcia,[3] Jan S. Bauer,[4] and Franz Pfeiffer[1,2]

[1]Physik-Department, Technische Universität München, James-Franck-Str. 1, 85748 Garching, Germany
[2]IMETUM Zentralinstitut für Medizintechnik, Technische Universität München, Boltzmannstraß e 11, 85748 Garching, Germany
[3]Institut für Radiologie, Klinikum rechts der Isar, Technische Universität München, Ismaninger Straße 22, 81675 München, Bavaria, Germany
[4]Abteilung für Neuroradiologie, Klinikum rechts der Isar, Technische Universität München, Ismaninger Straße 22, 81675 München, Bavaria, Germany

Abstract: The directional dark-field signal obtained with X-ray grating interferometry yields direction-dependent information about the X-ray scattering taking place inside the examined sample. It allows examination of its morphology without the requirement of resolving the micrometer size structures directly causing the scattering. The local morphology in turn gives rise to macroscopic mechanical properties of the investigated specimen. In this study, we investigate the relation between the biomechanical elasticity (Young's modulus) and the measured directional dark-field parameters of a well-defined sample made of wood. In our proof-of-principle experiment, we found a correlation between Young's modulus, the average dark-field signal, and the average dark-field anisotropy. Hence, we are able to show that directional dark-field imaging is a new method to predict mechanical sample properties. As grating interferometry provides absorption, phase-contrast, and dark-field data at the same time, this technique appears promising to combine imaging and mechanical testing in a single testing stage. Therefore, we believe that directional dark-field imaging will have a large impact in the materials science world.

Key words: grating interferometry, directional dark-field imaging, mechanical testing, Young's modulus, average anisotropy

INTRODUCTION

Finite element analysis is a well-established technique providing information about the mechanical properties of a specimen. However, it often requires high-resolution input data gained, for example, from micro computed tomography (microCT) measurements, which poses limits on the sample size. Directional dark-field imaging (Jensen et al., 2010a, 2010b) is a novel imaging technique that is based on the dark-field contrast provided by X-ray grating interferometry (Pfeiffer et al., 2008; Bech et al., 2010). It allows one to draw conclusions on the local orientation of the sample without directly resolving the corresponding structures (Wen et al., 2009; Yashiro et al., 2010; Lynch et al., 2011) and, thus, intrinsically allows coarser resolution and larger specimens. Directional dark-field imaging is not only feasible for thin specimens (Potdevin et al., 2012), but also for thicker ones where the resulting measured orientation resembles an average of overall structures passed by the X-ray beam (Revol et al., 2012; Malecki et al., 2013).

The basic principle behind directional dark-field imaging is as follows: as the grating interferometer is only sensitive to scattering occurring in directions perpendicular to the grating lines, the measured dark-field signal depends on the direction of the local scattering taking place inside the specimen. For an isotropic sample, the signal does not change with its relative orientation with respect to the interferometer. For an anisotropic specimen, however, the measured dark-field signal oscillates when rotating the specimen or the set-up around the optical axis. From these oscillations, the local mean amount of scattering, orientation, and anisotropy can be extracted. The resulting dark-field signal D with respect to the angle of rotation of the sample θ in detector pixel (m, n) can be described by (Jensen et al., 2010a, 2010b; Revol et al., 2012; Malecki et al., 2013):

$$D(m, n, \theta) = e^{-\{a(m,n)\cos[2(\theta - \phi(m,n))] + b(m,n)\}}. \quad (1)$$

The constant offset $b(m, n)$ provides information about the average signal upon rotation, which is equal to the average projected dark-field signal and therefore indirectly takes into account the sample thickness. It has been shown that, similar to absorption-based X-ray imaging, the dark-field signal follows an exponential decay with increasing sample thickness (Wang et al., 2009; Bech et al., 2010). The strength of the signal's dependency on the sample orientation is described by $a(m, n)$. The local degree of anisotropy DA is then defined with respect to the amplitude a and offset b of the oscillation by

$$DA(m, n) = \frac{a(m, n)}{b(m, n)}. \quad (2)$$

It is convenient to define the angles θ and ϕ with respect to the direction of the grating lines. Then, $\phi(m, n)$ specifies the local structure orientation.

Until now, most studies concerned with directional dark-field imaging only focused on features visible in the images (Jensen et al., 2010a, 2010b; Potdevin et al., 2012; Revol et al., 2013).

Here we show that the parameters gained from the directional dark-field signal are strongly linked to the material properties of the examined sample. We examined the mechanical stiffness of a wooden cube in combination with the average dark-field signal, the anisotropy, and the orientation derived from directional dark-field imaging.

MATERIALS AND METHODS

In principle, the directional dark-field imaging set-up contains a standard Talbot–Lau grating interferometer with a few special features making it dedicated for measurements at high energies in the hard X-ray region. The source was a high power X-ray tube source manufactured by COMET AG, Switzerland (MXR-160HP/11) operated at 60 kVp, 30 mA with a focal spot size of 1.0 mm^2. No filter was used for the measurements.

The gratings were manufactured by the Institute of Microstructure Technology, Karlsruhe Institute of Technology (KIT), and by Microworks GmbH. Out of the three gratings, two were absorption gratings (G_0 and G_2) with a silicon substrate height of 500 and 150 μm, respectively, and 160–170 μm high gold lines filled with SU-8 in between. The phase grating was fabricated of 8 μm high nickel lines on a 200 μm thick silicon substrate. A symmetric set-up geometry was chosen, which resulted in a magnification factor of two of the Talbot interference pattern. With the period of the phase grating of 5 μm and a phase shift of $\pi/2$ at the design energy of 46 keV, the absorption gratings had a period of 10 μm. Every grating had a duty cycle of 0.5 and the grating lines were oriented vertically. The inter-grating distances were 92.7 cm (first fractional Talbot distance). Stepping scans were performed by moving G_1, which was mounted on a Nanoconverter (Paul Scherrer Institute, 5232 Villigen PSI, Switzerland). As the detector we used a PaxScan 2520D with a CsI scintillator and a pixel pitch of 127 μm, manufactured by Varian Medical Systems, Inc. (Palo Alto, CA 94304, USA).

The directional dark-field scans were performed with 32 angular steps over 360° and at each angle, a phase stepping scan was performed over eight steps. Before and after each complete directional dark-field scan, a series of five flat-field images was recorded.

The sample was a wooden cube cut out of a cherry tree branch with an edge length of $3.0 \times 2.8 \times 2.8$ cm^3. Wood is a fibrous, hard material that has a specific structure. Trees grow by building a new fiber layer around the whole stem, building a ring-like structure which is therefore referred to as growth rings. This structure is usually built yearly and is also called an annual ring. These rings can be visually distinguished, because the wood grown in spring (earlywood) contains more vessels than the much denser wood grown in summer (latewood), which therefore appears darker (Koubaa et al., 2002; Kretschmann & Cramer, 2007). These growth rings are well visible in the photograph in Figure 1. Owing to its structure consisting of grains arranged in growth rings, wood is an orthotropic material, which is a special case of anisotropy. Wood has three mutually perpendicular axes (axial, radial, and circumferential) of rotational symmetry and has different properties (such as stiffness) along the grain and the two axes perpendicular to these fibers (Harrigan & Mann, 1984). The cutting directions were chosen such that they matched the grain direction as well as possible. Two of the surfaces were oriented perpendicular to the grain direction and the other four surfaces parallel to it.

For the directional dark-field measurements, the cube was placed 76 cm downstream from G_1, 22 cm in front of the detector. The sample stage was a sophisticated Eulerian cradle manufactured by Huber Diffraktionstechnik GmbH & Co. KG (83253 Rimsting, Germany). This goniometer allowed almost free rotation of the sample. As directional dark-field imaging is a radiographic technique, the cube was imaged along three different axes parallel to its face normals.

In order to visualize the cube's fiber structure directly, micro-tomography scans were performed with a v—tome—x s 240 microCT by GE Sensing & Inspection Technologies GmbH (85630 Grasbrunn/Neukeferloh, Germany). The resulting voxel size was 45.9 μm, the scan parameters were 60 kVp and 300 μA, the exposure time was 2,000 ms. 1,000 projections were recorded over an angular range of 360°.

The wooden cube was tested for its modulus of elasticity E (Young's modulus), which is a measure of stiffness of a material, with a Zwick mechanical testing system (Model 1120; Zwick Roell AG, Ulm, Germany). Three to four cycles of compression and decompression from 0 to 1,000 N were performed for each of the three tested axes. The stress–strain curves were recorded and the modulus of elasticity was calculated from these curves by dividing the slope of each curve by the cross-sectional area on which the stress was applied. The curves were not linear from the beginning because of the preconditioning. The results were averaged over all cycles and are given in Table 1. In addition, the error for the stress–strain tests needs to be assessed as roughly 10%.

RESULTS

Figures 1b–1d show three orthogonal planes through the reconstructed volume of the wooden cube gained from the microCT measurements. The orientation of the wooden fibers is clearly visible. In b and c, the fibers are more or less oriented along the z direction, which is along the growth direction of the branch. Figure 1d shows a slice perpendicular to the former two, where it becomes visible that the fibers are aligned concentrically around the branch direction.

The corresponding directional dark-field images are shown in Figure 1. As in previous works (cf. e.g., Potdevin et al., 2012), the structure orientation and the anisotropy are encoded in color in Figures 2a–2c. The saturation
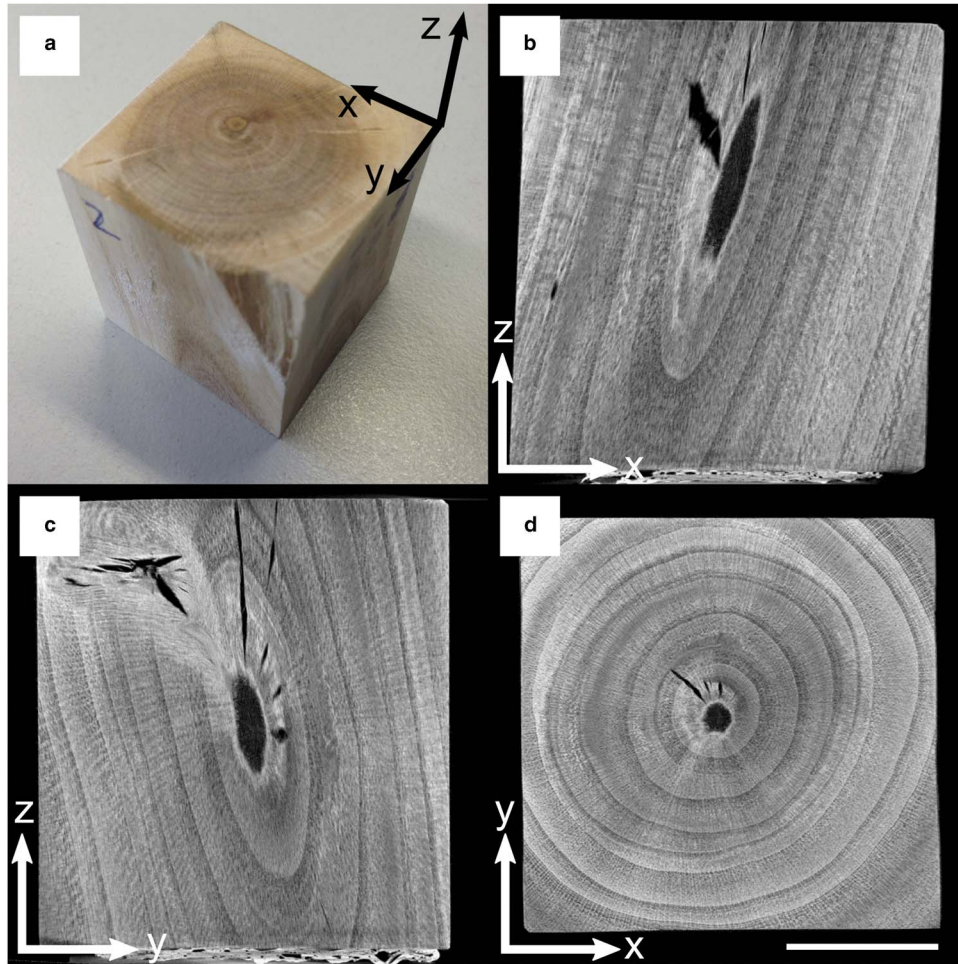
Figure 1. The wooden cube sample was cut out of a cherry tree branch. **a:** Photograph of the specimen demonstrating the chosen coordinate system. The cube had an edge length of 3 cm. **b–d:** Example micro-tomography slices through the cube volume showing the strong local orientation of the wood fibers. Scale bar is 1 cm.

corresponds to the anisotropy and the hue specifies the direction. By comparing the directly resolved fiber orientations of the microCT data to the orientation derived from directional dark-field imaging, one can clearly see that they agree qualitatively. Figures 2d–2f show the mean dark-field signal with respect to the rotation of the sample around the optical axis, whereas Figures 2g–2i depict the local anisotropy. Obviously, the mean dark-field signal is significantly stronger along direction z than along x and y. By contrast, the

local anisotropy dominates in those projections taken along the x and y direction. To examine the relation of the elasticity represented by the Young's modulus to the parameters gained from directional dark-field imaging, we extracted the mean logarithmic dark-field values $\overline{-\ln D}$, anisotropies $\overline{DA}$, and orientations $\overline{\phi}$ for the regions of interest marked in Figures 2a–2c, and calculated their variance. The mean values were calculated according to

$$\overline{\ln D} = \frac{1}{A_{\text{ROI}}} \sum_{\text{ROI}} b(m, n), \tag{3}$$

$$\overline{DA} = \frac{1}{A_{\text{ROI}}} \sum_{\text{ROI}} DA(m, n), \tag{4}$$

$$\overline{\phi} = \frac{1}{2} \text{Im} \ln \frac{\sum_{\text{ROI}} DA(m, n) \exp[2i\phi(m, n)]}{\sum_{\text{ROI}} DA(m, n)}, \tag{5}$$

where A_{ROI} is the area of each region of interest (ROI) in detector pixels, respectively. For $\overline{\phi}$, the average was weighted by the degree of anisotropy.

Table 1. Experimental Data Gained from Directional Dark-Field Imaging and Biomechanical Testing of the Wooden Cube.

Direction	E (kN/mm^2)	$\overline{-\ln D}$	$\overline{DA}$	$\overline{\phi}$
x	0.78 ± 0.08	1.0 ± 0.2	0.38 ± 0.08	$-5.9 \pm 3.7°$
y	1.10 ± 0.11	1.0 ± 0.3	0.32 ± 0.06	$13.6 \pm 3.5°$
z	2.47 ± 0.25	2.9 ± 0.4	0.23 ± 0.09	$62.3 \pm 29.8°$

Shown are the E modulus, the average logarithmic dark-field signal $\overline{-\ln D}$, the mean degree of anisotropy $\overline{DA}$, and the average orientation $\overline{\phi}$ averaged over the region of interests shown in Figure 2.
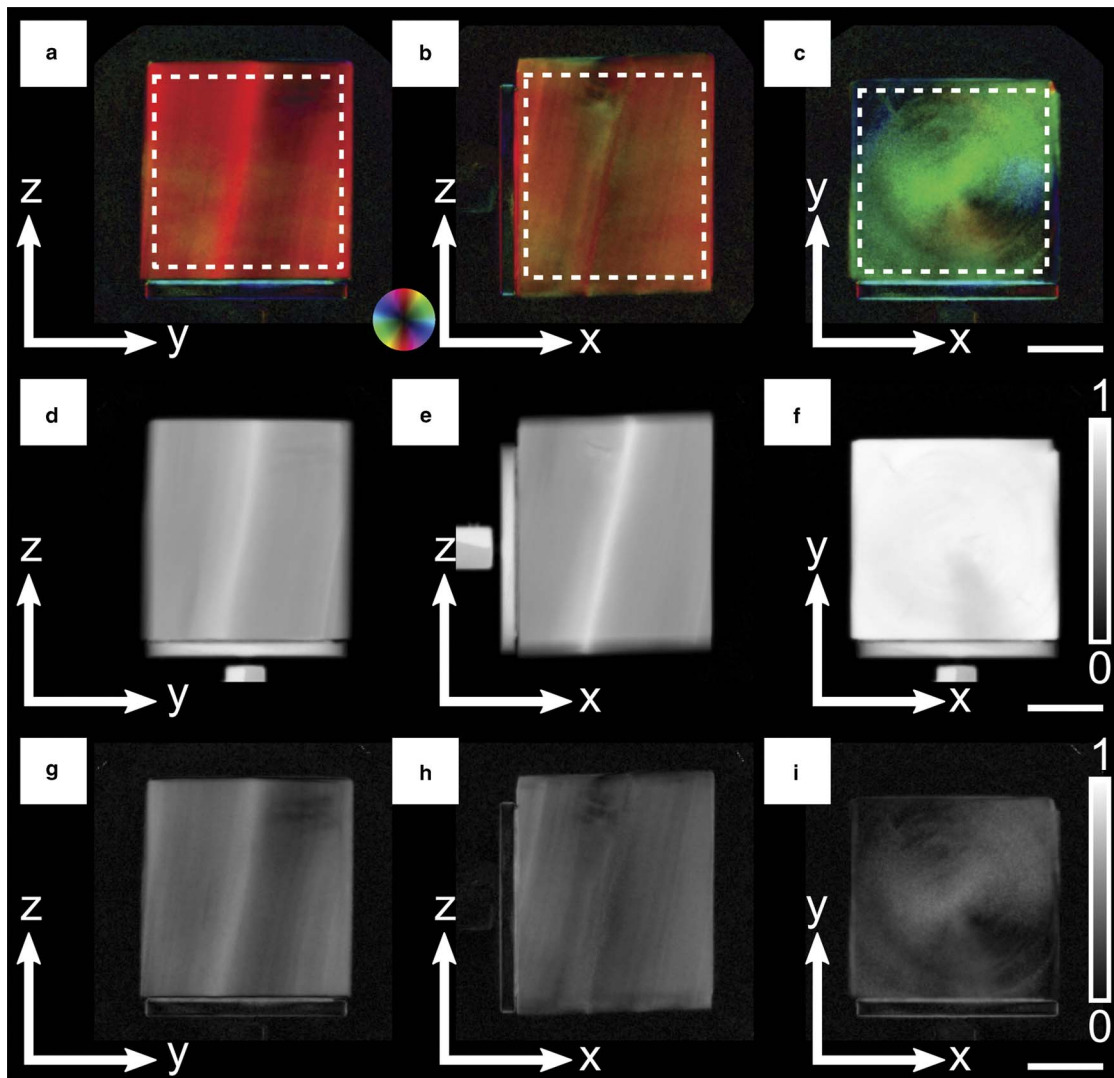
Figure 2. Visualizization of the directional dark-field data of the wooden cube. The sample was mounted on a PMMA dish, which is visible as well. **a–c:** Dark-field X-ray radiographs showing orientation and anisotropy. The color specifies the local orientation, whereas the brightness encodes the local anisotropy. The orientation is extracted from the maxima/minima of the scattering signal. The anisotropy corresponds to the degree of fiber orientation. In (**a**) and (**b**), the wood fibers are oriented approximately along the z direction; (**c**) shows the cube along the z axis, where it has a preferred orientation along the diagonal between the y and x directions. For a quantitative analysis, the average anisotropy and the average mean dark-field signal were calculated for all three orientations over the indicated areas. **d–f:** Mean dark-field projections giving the average scattering with respect to the rotation around the optical axis. The average scattering is related to the fiber density inside the specimen. **g–i:** Anisotropy images showing the anisotropy in the recorded scattering signal upon rotation. Scale bar is 1 cm.

The direction angles were measured clockwise with respect to the vertical axis in every directional dark-field projection. The results for each quantity are shown in Table 1 and are plotted in Figure 3. A correlation can be seen for the displayed quantities. The correlation coefficients were calculated as $R = 0.984$ for dark field and $R = -0.975$ for anisotropy.

DISCUSSION

This study demonstrated a strong relationship between mechanical properties and measures of anisotropy as revealed by directional dark-field imaging. The fiber orientation found in the microtomographic slices corresponds well with the expected structures caused by the growth process of the wood. We therefore expected the scattering inside the sample to be highly anisotropic and to produce a well-defined directional dark-field signal. The orientation $\overline{\phi}$ derived from directional dark-field imaging also agrees with the fiber orientation inside the sample. For the radiographs along the x direction, the preferred orientation is well defined and deviates from the vertical direction by $\sim 6°$. The same is true along the y direction, where the deviation is $\sim 14°$. Along the z direction, the orientation shows a large variation, but an average orientation of 62° is caused by the prominent diagonal structure with
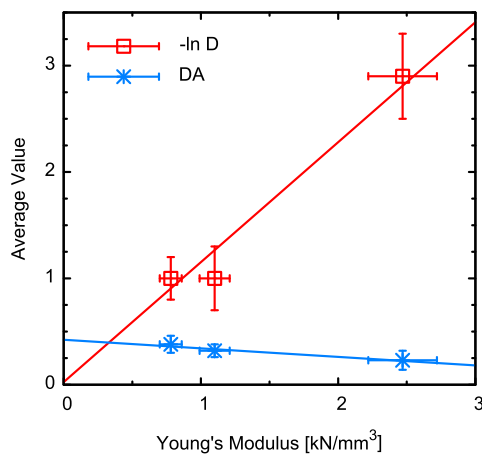
Figure 3. Plot of dark-field data against Young's modulus. The mean logarithmic dark-field signal $\overline{-\ln D}$ is shown in red, the anisotropy $\overline{DA}$ in blue. Both quantities are correlated to the Young's modulus E. The average logarithmic dark-field signal is positively correlated ($R = 0.984$) and the mean anisotropy shows a negative correlation ($R = -0.975$) to the E modulus. The corresponding line fits are shown by dashed lines.

higher anisotropy than in the remaining sample. This can be seen in Figures 2c & 2i.

Wood is stiffer when stress is applied parallel to the direction of the fibers (along z) than when it is applied perpendicular to the direction of the wood fibers (along x or y). In principle, a tree branch should behave isotropically for radial pressure because of its orthotropic structure, i.e., for directions perpendicular to the grain direction (if there are no knots or other branches emerging). We ascribe the slight difference in Young's modulus between directions x and y to the fact that the fiber orientation slightly deviates from the x direction.

Moreover, the quantitative statistical comparison of the dark-field data to the mechanical properties of the wooden cube confirms the expectations from the orthotropic nature of wood. Young's modulus E, average logarithmic dark-field signal $\overline{-\ln D}$, and average anisotropy $\overline{DA}$ are strongly correlated. With increasing stiffness, the average logarithmic dark-field signal increases[a] and the average anisotropy decreases. This implies that strong scattering and the lack of a preferred scattering orientation add stiffness to a structure. This corresponds on the one hand to a large number of micrometer size structures and on the other to an isotropic morphology transverse to the viewing direction. It is of importance to note that, even though the individual structures are much smaller than the pixel size of the detector used for the directional dark-field measurement, information about them can be obtained.

CONCLUSIONS

In conclusion, we were able to show that the mechanical stiffness of our sample is correlated to parameters provided

---

[a] This means lower values for the measured dark-field signal D.

by directional dark-field imaging. The average dark-field signal is related to the fiber density, and the scattering anisotropy corresponds to the degree of fiber orientation. The main scattering direction provides information about the main fiber orientation with both directions being orthogonal with respect to each other. Consequently, a higher average dark-field signal $\overline{-\ln D}$ is equivalent to a higher Young's modulus. The more anisotropic the structures appear with respect to directional dark-field imaging, the lower is their stiffness. We are convinced that similar results can be obtained for a statistically relevant number of samples and even for less well-defined samples in both materials science as well as the biomedical field.

REFERENCES

BECH, M., BUNK, O., DONATH, T., FEIDENHANS'L, R., DAVID, C. & PFEIFFER, F. (2010). Quantitative X-ray dark-field computed tomography. *Phys Med Biol* **55**(18), 5529–5539.

HARRIGAN, T.P. & MANN, R.W. (1984). Characterization of microstructural anisotropy in orthotropic materials using a second rank tensor. *J Mater Sci* **19**(3), 761–767.

JENSEN, T.H., BECH, M., BUNK, O., DONATH, T., DAVID, C., FEIDENHANS'L, R. & PFEIFFER, F. (2010a). Directional X-ray dark-field imaging. *Phys Med Biol* **55**(12), 3317–3323.

JENSEN, T.H., BECH, M., ZANETTE, I., WEITKAMP, T., DAVID, C., DEYHLE, H., RUTISHAUSER, S., REZNIKOVA, E., MOHR, J., FEIDENHANS'L, R. & PFEIFFER, F. (2010b). Directional X-ray dark-field imaging of strongly ordered systems. *Phys Rev B* **82**(21), 214103.

KOUBAA, A., ZHANG, S.Y.T. & MAKNI, S. (2002). Defining the transition from earlywood to latewood in black spruce based on intra-ring wood density profiles from X-ray densitometry. *Ann Forest Sci* **59**(5–6), 511–518.

KRETSCHMANN, D.E. & CRAMER, S.M. (2007). The role of earlywood and latewood properties on dimensional stability of loblolly pine. Proceedings of the Compromised Wood Workshop, Christchurch, NZ, School of Forestry, Wood Technology Research Centre, January 29–30, University of Canterbury, pp. 215–236.

LYNCH, S.K., PAI, V., AUXIER, J., STEIN, A.F., BENNETT, E.E., KEMBLE, C.K., XIAO, X., LEE, W.-K., MORGAN, N.Y. & HAROLD WEN, H. (2011). Interpretation of dark-field contrast and particle-size selectivity in grating interferometers. *Appl Opt* **50**(22), 4310–4319.

MALECKI, A., POTDEVIN, G., BIERNATH, T., EGGL, E., GRANDE GARCIA, E., BAUM, T., NOËL, P.B., BAUER, J.S. & PFEIFFER, F. (2013).

Coherent superposition in grating-based directional dark-field imaging. *PLoS One* **8**(4), e61268.

PFEIFFER, F., BECH, M., BUNK, O., KRAFT, P., EIKENBERRY, E.F., BRÖNNIMANN, C., GRÜNZWEIG, C. & DAVID, C. (2008). Hard-X-ray dark-field imaging using a grating interferometer. *Nat Mater* **7**(2), 134–137.

POTDEVIN, G., MALECKI, A., BIERNATH, T., BECH, M., JENSEN, T.H., FEIDENHANS'L, R., ZANETTE, I., WEITKAMP, T., KENNTNER, J., MOHR, J., ROSCHGER, P., KERSCHNITZKI, M., WAGERMAIER, W., KLAUSHOFER, K., FRATZL, P. & PFEIFFER, F. (2012). X-ray vector radiography for bone micro-architecture diagnostics. *Phys Med Biol* **57**(11), 3451–3461.

REVOL, V., KOTTLER, C., KAUFMANN, R., NEELS, A. & DOMMANN, A. (2012). Orientation-selective X-ray dark field imaging of ordered systems. *J Appl Phys* **112**(11), 114903.

REVOL, V., PLANK, B., KAUFMANN, R., KASTNER, J., KOTTLER, C. & NEELS, A. (2013). Laminate fibre structure characterisation of carbon fibre-reinforced polymers by X-ray scatter dark field imaging with a grating interferometer. *NDT & E International* May, 64–71.

WANG, Z.-T., KANG, K.-J., HUANG, Z.-F. & CHEN, Z.-Q. (2009). Quantitative grating-based X-ray dark-field computed tomography. *Appl Phys Lett* **95**(9), 094105.

WEN, H., BENNETT, E.E., HEGEDUS, M.M. & RAPACCHI, S. (2009). Fourier X-ray scattering radiography yields bone structural information. *Radiology* **251**(3), 910–918.

YASHIRO, W., TERUI, Y., KAWABATA, K. & MOMOSE, A. (2010). On the origin of visibility contrast in X-ray Talbot interferometry. *Opt Expr* **18**(16), 16890–16901.